Measuring the evolution of the most stable optical clock G 117-B15A

S.O. Kepler, J.E.S. Costa, B.G. Castanheira

Instituto de Física da UFRGS, 91501-900 Porto Alegre, RS - Brazil, kepler@if.ufrgs.br

D.E. Winget, Fergal Mullally, R.E. Nather, Mukremin Kilic & Ted von Hippel

Department of Astronomy and McDonald Observatory, University of Texas, Austin, TX 78712 - U.S.A.

Anjum S. Mukadam

Department of Astronomy, University of Washington, Seattle, WA - 98195-1580, U.S.A.

Denis J. Sullivan

School of Chemical And Physical Sciences, Victoria University of Wellington, New Zealand

ABSTRACT

We report our measurement of the rate of change of period with time ($\dot{P}$) for the 215 s periodicity in the pulsating white dwarf G 117–B15A, the most stable optical clock known. After 31 years of observations, we have finally obtained a $4\,\sigma$ measurement $\dot{P}_{\rm observed} = (4.27 \pm 0.80) \times 10^{-15}$ s/s. Taking into account the proper-motion effect of $\dot{P}_{\rm proper} = (7.0 \pm 2.0) \times 10^{-16}$ s/s, we obtain a rate of change of period with time of $\dot{P} = (3.57 \pm 0.82) \times 10^{-15}$ s/s. This value is consistent with the cooling rate in our white dwarf models only for cores of C or C/O. With the refinement of the models, the observed rate of period change can be used to accurately measure the ratio of C/O in the core of the white dwarf.

Subject headings: Stars: evolution – stars: oscillations – stars: individual: G 117-B15A

1. Introduction

G 117–B15A is a pulsating white dwarf with a hydrogen atmosphere, a DAV, also called a ZZ Ceti star (McGraw 1979). These stars show multi-periodic non-radial g-mode pulsations that can be used to measure their internal properties and rate of evolution.

McGraw & Robinson (1976) found the star was variable, and Kepler et al. (1982) studied its light curve, finding 6 simultaneous pulsations. The dominant mode has a period of 215 s, a fractional amplitude of 22 mma (milli-modulation amplitude = 1/1.086 milli magnitude), and is stable in amplitude and phase. The other smaller pulsation modes vary in amplitude from night to night (Kepler et al. 1995), suggesting the presence of unresolved components. Because the DAVs appear to be normal stars except for their variability (Robinson 1979; Bergeron et al. 1995, 2004), i.e., an evolutionary stage in the cooling of all white dwarfs, it is likely that the DAV structural properties are representative of *all* DA white dwarfs.

Mukadam et al. (2004a) and Mullally et al. (2005) discovered 46 new ZZ Cetis and more than doubled the number of known variables, using $T_{\rm eff}$ and log g values derived from the optical spectra obtained by the Sloan Digital Sky Survey (Kleinman et al. 2004). While Bergeron et al. (1995, 2004) find the ZZ Ceti instability strip to be pure, i.e., contain no non-variable stars, Mukadam et al. (2004a,b); Mullally et al. (2005) find several stars inside the instability strip for which they could detect no variability above their detection threshold. It is necessary to obtain $S/N \geq 50$ spectra of the non-variables within the strip and re-analyze their $T_{\rm eff}$ and log g values, and also to obtain additional time series photometry on these stars, to ensure that they are not low amplitude variables, and re-study the purity of the instability strip.

We report our continuing study of the star G 117–B15A, also called RY LMi and WD 0921+354, one of the hottest of the ZZ Ceti stars. We expect that the rate of change of a pulsation period with time for g-mode pulsations in white dwarf stars to be directly related to its evolutionary timescale (Winget et al. 1983), allowing us to infer the age of a cool white dwarf since its formation. We have been observing the star since 1974 to measure the rate of period change with time ($\dot{P}$) for the largest amplitude periodicity. Using all the data obtained from 1974 through 1999, Kepler et al. (2000) arrived at a determination of $\dot{P} = (2.3 \pm 1.4) \times 10^{-15}$ s/s.

G 117–B15A was the first pulsating white dwarf to have its main pulsation mode index identified. The 215 s mode is an $\ell = 1$, as determined by comparing the ultraviolet pulsation amplitude (measured with the Hubble Space Telescope) to the optical amplitude (Robinson et al. 1995). Kotak et al. (2004) confirm the ℓ measurement for the P=215 s pulsation, and show that the other large amplitude modes, at 271 s and 304 s, show chromatic amplitude changes that do not fit the theoretical models, using time-resolved spectra obtained at the Keck Telescope. Robinson et al. (1995), and Koester, Allard, & Vauclair (1994) derive $T_{\rm eff}$ near 12,400 K, while Bergeron et al. (1995, 2004) using a less efficient model for convection, derive $T_{\rm eff}$=11,630 K.

Kepler (1984) demonstrated that the observed variations in the light curve of G 117–

B15A are due to non-radial g-mode pulsations. Kepler et al. (2000) show the models predict the effect of radius change due to still ongoing contraction to be an order of magnitude smaller than the cooling effect on the rate of period change.

G 117–B15A is proving to be a useful laboratory for particle physics (Isern et al. 2004). Corsico et al. (2001) calculated the limit on the axion mass compatible with the then observed upper limit to the cooling, showing $m_a \cos\beta \leq 4.4$ meV and Kepler (2004) demonstrates axion cooling would be dominant over neutrino cooling for the lukewarm white dwarf stars for axion masses of this order. Biesiada & Malec (2002) show that the 2σ upper limit published in Kepler et al. (2000) limits the string mass scale $M_S \geq 14.3$ TeV/c^2 for 6 dimensions, from the observed cooling rate and the emission of Kaluza-Klein gravitons, but the limit is negligible for higher dimensions. Benvenuto et al. (2004) show the observed rates of period change can also be used to constrain the dynamical rate of change of the constant of gravity $\dot{G}$.

Bradley (1996, 1998) used the mode identification and the observed periods of the 3 largest known pulsation modes to derive a hydrogen layer mass lower limit of $10^{-6}\,M_*$, and a best estimate of $1.5 \times 10^{-4}\,M_*$, assuming $k = 2$ for the 215 s mode, and 20:80 C/O core mass. The core composition is constrained mainly by the presence of the 304 s pulsation. Benvenuto et al. (2002) show the seismological models with time-dependent element diffusion are only consistent with the spectroscopic data if the modes are the $\ell = 1$, k=2, 3, and 4, and deduces $M = 0.525\ M_\odot$, $\log(M_H/M_*) \geq -3.83$ and $T_{\rm eff} = 11\,800$ K. Their best model predicts: parallax Π=15.89 mas, $\dot{P} = 4.43 \times 10^{-15}$ s/s, for the P=215 s, $\dot{P} = 3.22 \times 10^{-15}$ s/s, for the P=271 s, and $\dot{P} = 5.76 \times 10^{-15}$ s/s, for the P=304 s periodicities.

2. Observations

Kepler et al. (2000) reported on the observations from 1974 to 2000. We report in this paper additional 19.3 h of time series photometry in 2001, 30.6 h in 2002, 24.4 h in 2003, 4 h in 2004, and 13.6 h in 2005, most using the Argos prime-focus CCD camera (Nather & Mukadam 2004) on the 2.1 m Otto Struve telescope at McDonald Observatory.

We observed the light through a BG40 filter to maximize the signal-to-noise ratio (S/N) because the pulsation amplitudes are small (2%), the star is faint (V=15.52, Eggen & Greenstein 1965), and also because the non-radial g-mode light variations have the same phase in all colors (Robinson, Kepler, & Nather 1982) but the amplitudes decrease with wavelength. For example, a filter-less observation with Argos gives an amplitude around 40% smaller for G 117–B15A.

3. Data Reduction

We reduce and analyze the data in the manner described by Nather et al. (1990), and Kepler (1993). We bring all the data to the same fractional amplitude scale, and the times from UTC to the uniform Barycentric Julian Coordinated Date (TCB) scale, using JPL DE405 ephemeris (Standish 1998, 2004) to model Earth's motion. We compute Fourier transforms for each individual run, and verify that the main pulsation at 215 s dominates each data set and has an amplitude stable up to 15%, our uncertainty in amplitude due to the lack of accurate time- and color-dependent extinction determination.

4. Time Scale for Period Change

As the dominant pulsation mode at P=215 s has a stable frequency and amplitude since our first observations in 1974, we can calculate the time of maximum for each new run and look for deviations.

We fit our observed time of maximum light to the equation:

$$(O-C) = \Delta E_0 + \Delta P \cdot E + \frac{1}{2} P \cdot \dot{P} \cdot E^2$$

where $\Delta E_0 = (T^0_{max} - T^1_{max})$, $\Delta P = (P - P_{t=T^0_{max}})$, E is the epoch of the time of maximum, i.e, the integer number of cycles after our first observation, T^0_{max} is the time of maximum assumed, T^1_{max} is the time of maximum that best fit the parabola, P is the period that best fit the parabola, and $P_{t=T^0_{max}}$ is the period assumed at T^0_{max} [1]. The times of maxima are calculated by a linear least-squares fit of the light curve of each night to a sum of the six detected frequencies. They are shown in Table 6.

In Figure 1, we show the O–C timings after subtracting the correction to period and epoch, and our best fit curve through the data. The size of each point is proportional to its weight, i.e., inversely proportional to the square of uncertainty in phase. The error bars plotted are $\pm 1\sigma$. From our data through 2005, we obtain a new value for the epoch of maximum, $T^0_{max} = 244\,2397.9175141\,\mathrm{TCB} \pm 0.41\,\mathrm{s}$, a new value for the period, $P = 215.1973888 \pm 0.0000004\,\mathrm{s}$, and most importantly, a rate of period change of:

$$\dot{P} = (4.27 \pm 0.80) \times 10^{-15}\,\mathrm{s/s}.$$

[1] Fitting the whole light curve with a term proportional to $\sin\left[\frac{2\pi}{(P+\frac{1}{2}\dot{P})}t + \phi\right]$ by non-linear least squares gives unreliable uncertainty estimates and the alias space in P and $\dot{P}$ is extremely dense due to 31 yr data set span (O'Donoghue 1994; Costa et al. 1999). Our non-linear least squares result is $\dot{P} = (3.38 \pm 0.0013) \times 10^{-15}$s/s.

We use linear least squares to make our fit, with each point weighted inversely proportional to the uncertainty in the time of maxima for each individual run squared. We quadratically add an additional 1s of uncertainty to the time of maxima for each night to account for external uncertainty caused perhaps by the beating of possible small amplitude pulsations (Kepler et al. 1995) or the small modulation seen in Figure 1. The amplitude, 1s, is chosen from the Fourier transform of the (O-C) shown in Figure 2, and is in agreement with Kopeikin & Potapov (2004) conclusion that the Fourier analysis of the Times of Arrival (TOA) gives unbiased information about the noise. Such external uncertainty is also consistent with Splaver et al. (2005) who show that the true uncertainties of the times of arrival of the milli-second pulsars are generally larger than the formal uncertainties, and that a quadratic term is added to them to fit the observations.

5. Discussion

While it is true that the period change timescale can be proportional to the cooling timescale, it is also possible that other phenomena with shorter timescales can affect $\dot{P}$. The cooling timescale is the longest possible one.

As a corollary, if the observed $\dot{P}$ is low enough to be consistent with evolution, then other processes, such as perhaps a magnetic field or diffusion induced changes in the boundary layers, are not present at a level sufficient to affect $\dot{P}$.

For the first time we also report on the search for the rates of period changes for the other relatively large amplitude modes of G 117–B15A, $dP/dt = (36.0 \pm 7.2) \times 10^{-15}$ s/s for the 270s periodicity, and $dP/dt = (74 \pm 15) \times 10^{-15}$ s/s for the 304s periodicity. They are much larger than the one derived for the main pulsation, which has a region of period formation deeper in the core, but are in line with the measurements for the 274s modes in ZZ Ceti (Mukadam et al. 2003). The models to date, without rotation, differential rotation, and magnetic fields, do not explain such values, or the chromatic amplitude changes reported by Kotak et al. (2004). Kepler et al. (1995) show the 270s and 304s periodicities have significant amplitude changes, indicative of multiple components or resonances.

5.1. Theoretical Estimates and Corrections

5.1.1. Proper Motion

Pajdosz (1995) discusses the influence of the proper motion of the star on the measured

$\dot{P}$:

$$\dot{P}_{\rm obs} = \dot{P}_{\rm evol}\,(1 + v_r/c) + P\dot{v}_r/c$$

where v_r is the radial velocity of the star. Assuming $v_r/c \ll 1$ he derived

$$\dot{P}_{\rm pm} = 2.430 \times 10^{-18} P[s]\,(\mu[\text{"}/yr])^2\,d[\rm pc]$$

where $\dot{P}_{\rm pm}$ is the effect of the proper motion on the rate of period change, P is the pulsation period, μ is the proper motion and d is the distance. The proper motion, $\mu = 0.136 \pm 0.002$"/yr, and the parallax, $\Pi = (0.0105 \pm 0.004)$", are given by van Altena et al. (1995). But the parallax has a large uncertainty and does not agree with other estimates of the distance. Munn et al. (2004) measured the same proper motion for G 117-B15A and G 117-B15B: $\mu_\alpha = (-146 \pm 2.6)$ mas/yr, and $\mu_\delta = (-1.0 \pm 2.6)$ mas/yr, including 5 USNO-B epochs and SDSS positions. Considering $V^A = 15.50 \pm 0.02$ (Silvestri et al. 2002), if we use Bergeron et al. (2004) estimate of $M_V^A = 11.70 \pm 0.06$[2] derived from their optical spectra, we obtain a distance of 58 ± 2 pc, equivalent to a spectroscopic parallax of 0.0172 ± 0.0005". But G 117-B15A has International Ultraviolet Explorer (IUE) and Hubble Space Telescope (HST) Faint Object Spectrograph (FOS) flux calibrated spectra (Koester, Allard, & Vauclair 1994) that can also be used to estimate the distance, if we use the evolutionary models of Wood (1995) or Panei et al. (2000) to estimate the radius from $T_{\rm eff}$ and $\log g$ and fit the observed fluxes to a model atmosphere calculated by Detlev Koester, similar to that described in Finley et al. (1997), but with an ML2/α=0.6 convection description consistent with Bergeron et al. (1995) and Koester & Holberg (2001). The IUE spectra re-calibrated according to the New Spectroscopic Image Procession System (NEWSIPS) data reduction by NASA was published by Holberg, Barstow, & Burleigh (2003). From the IUE spectra we get a distance of $d = 59 \pm 6$ pc. The HST spectra, shown in Figure 3, fits a distance of $d = 67 \pm 5$ pc. Table 1 lists all the available distances to G 117-B15A.

Taking the average value of proper motion and distance, we estimate

$$\dot{P}_{\rm pm} = (7.0 \pm 2.0) \times 10^{-16}\,{\rm s/s}$$

and

$$\dot{P} = \dot{P}_{\rm observed} - \dot{P}_{\rm pm} = (3.57 \pm 0.82) \times 10^{-15}\,{\rm s/s}$$

[2]We estimate the uncertainty in the absolute magnitude from the 300 K external uncertainty in Bergeron's temperatures.

Table 1: G 117-B15A distance determinations

Method	**distance (pc)**
Parallax	95 ± 37
Spectroscopic parallax	58 ± 2
IUE flux	59 ± 5
HST flux	67 ± 4
Seismology from Bradley (1998)	61
Seismology from Benvenuto et al. (2002)	63
Mean	67 ± 14

5.2. Pulsation Models

We compare the measured value of $\dot{P}$ with the range of theoretical values derived from realistic evolutionary models with C/O cores subject to g–mode pulsations in the temperature range of G 117–B15A. The adiabatic pulsation calculations of Bradley (1996), and Brassard et al. (1992, 1993), which allow for mode trapping, give $\dot{P} \simeq 2 - 7 \times 10^{-15}$ s/s for the $\ell = 1$, low k oscillation observed. Benvenuto et al. (2004) estimated the theoretical $\dot{P}$ for the three modes of G 117-B15A, even allowing for a dynamical change on the gravity constant, as we show in section 1. The observed $P/\dot{P} = 1.9 \times 10^9$ yr, equivalent to 1 s change in period in 8.9 million years, is within the theoretical predictions and very close to it. We have therefore measured a rate consistent with the evolutionary time scale for this lukewarm white dwarf.

5.2.1. Core Composition

For a given mass and internal temperature distribution, theoretical models show that the rate of period change increases if the mean atomic weight of the core is increased, for models which have not yet crystallized in their interiors. As the evolutionary model cools, its nucleus crystallizes due to Coulomb interactions between the ions (Lamb & van Horn 1975), and crystallization slows down the cooling by the release of latent heat. Montgomery & Winget (1999) describe the effect of crystallization on the pulsations of white dwarf stars, but G 117–B15A is not cool enough to have a crystallized core (Winget et al. 1997), or even for the convective coupling described by Fontaine et al. (2001) to occur.

The heavier the particles that compose the nucleus of the white dwarf, the faster it cools. The best estimate of mean atomic weight A of the core comes from the comparison of the

observed $\dot{P}$ with values from an evolutionary sequence of white dwarf models. Brassard et al. (1992) computed the rates of period changes for 800 evolutionary models with various masses, all with carbon cores but differing He/H surface layer masses, obtaining values similar to those of Winget et al. (1981), Wood & Winget (1988), and Bradley & Winget (1991). The average value of $\dot{P}$ for all $\ell = 1$, 2 and 3 modes with periods around 215 s in models with an effective temperature around 13,000 K, and a mass of 0.5 $M_{\odot}$, is: $\dot{P}$(C core) = $(4.3 \pm 0.5) \times 10^{-15}$ s/s. Benvenuto et al. (2004) C/O models give $\dot{P}$(C/O core) = $(3-4) \times 10^{-15}$ s/s. Using a Mestel-like cooling law (Mestel 1952; Kawaler et al. 1986), i.e., $\dot{T} \propto A$, where A is the mean atomic weight in the core, we can write:

$$\dot{P}(A) = (3-4) \times 10^{-15} \frac{A}{14} \text{ s/s.}$$

The observed rate of period change is therefore consistent with a C or C/O core. The largest uncertainty comes from the models.

5.2.2. Reflex Motion

The presence of an orbital companion could contribute to the period change we have detected. When a star has an orbital companion, the variation of its line-of-sight position with time produces a variation in the time of arrival of the pulsation maxima, by changing the light travel time between the star and the observer by reflex motion of the white dwarf around the barycenter of the system. Kepler et al. (1991) estimated a contribution to $\dot{P}$ caused by reflex orbital motion of the observed proper motion companion of G 117–B15A in their equation (10) as:

$$\dot{P}_{\rm orbital} = \frac{P_{\rm pul}}{c} \frac{GM_B}{a_T^2} = 1.97 \times 10^{-11} P_{\rm pul} \frac{M_B/M_{\odot}}{(a_T/AU)^2} \text{ s/s}$$

where a_T is the total separation and M_B is the mass of the companion star. In the above derivation they have also assumed the orbit to be nearly edge on to give the largest effect possible. Only the acceleration term parallel to the line of sight contributes to $\dot{P}$. Even though G 117-B15A and G 117–B15B are a common proper motion pair (Giclas et al. 1963; van Altena et al. 2001), there is no other evidence they form a real binary system. Kotak et al. (2004) classifies G 117-B15B as an M3Ve from its spectra, obtained with the 10 m Keck I telescope, and measured $\log g \simeq 4.5$ and $T_{\rm eff} \simeq 3400$ K. With $V^B = 16.1$ (Harrington & Dahn 1980; van Altena et al. 2001) and $M_V^B \simeq 10.4 \pm 0.9$ (Lang 1991) with the uncertainty coming from a possible misclassification in the spectral type of G 117–B15B from M3V to M4V. Such uncertainty arises from the TiO and CaOH bands seen by Kotak et al. (2004) and the (B-V)=1.63 (Harrington & Dahn 1980). Its spectroscopic distance

is $d^B = 138 \pm 47$ pc. G 117-B15B is chromospherically active (Kotak et al. 2004) and a flare star (Nather & Mukadam 2004). G 117-B15A and B were imaged by SDSS DR3, with $u_A = 15.92$, $g_A = 15.54$, $r_A = 15.64$, $i_A = 15.80$, $z_A = 16.06$, and $u_B = 19.38$, $g_B = 16.95$, $r_B = 15.46$, $i_B = 13.97$, $z_B = 13.16$, which also measure a separation of 13.4". They were also observed by 2MASS (Cutri et al. 2003), with $J_A = 15.599 \pm 0.065$, $H_A = 15.614 \pm 0.12$, and $J_B = 11.599 \pm 0.018$, $H_B = 11.156 \pm 0.12$, and separation of 13.4". Using Pickles (1998) main sequence spectral templates convolved with SDSS filters, our best fitting template is an M4V, with $M_V^B = 11.54$, and a distance of 82 pc. Using Hawley et al. (2002) calibration for the infrared colors, G 117-B15B is consistent with the M3V spectral type, and the (i-z) colors correspond to $M_i^B = 10.33$, and a distance of 54 parsecs. Using the (i-J) colors, $M_J^B = 10.05$, we obtain a distance of 61 parsecs. The parallaxes $\pi^A = 11 \pm 5$ mas, $\pi^B = 5 \pm 7$ mas (van Altena et al. 2001), and $\pi^B = 4 \pm 7$ mas (Harrington & Dahn 1980) are too uncertain to be used to study the binary nature. Table 2 lists all the available distances to G 117-B15B. The mass of an M3.5V should be around $(0.30 \pm 0.03)\ M_\odot$ (Lang 1991).

Method	**distance (pc)**
Parallax	200 ± 280
Spectroscopic parallax	138 ± 47
SDSS colors	82
(i-z) colors	54
(i-J) colors	61
Mean	107 ± 62

Table 2: Distance determinations to G 177-B15B

With a separation around 13.4 arcsec $a_T = (898 \pm 188)$ AU, corresponding to an orbital period around $(28\,500 \pm 2200)$ years, we get $\dot{P}_{\rm orbital} \leq (1.6 \pm 1.6) \times 10^{-15}$ s/s. The large uncertainty takes into account the possibility the orbit might be strongly elliptical. Greaves (2004), in his section 4.3.1, discusses common proper motion pairs which possibly do not form a physical binary. If G 117–B15A and B form a real binary system, the contribution of an orbital reflex motion to the observed $\dot{P}$ might account for one half of the observed $\dot{P}$.

The whole observed rate of period change *could* also be caused by a planet of Jupiter's mass orbiting the white dwarf at a distance of 31 AU, which corresponds to an orbital period of 223 yr, or a smaller planet on a closer orbit (see Figure 4). A planet with Jupiter's mass any closer to the white dwarf would lead to a larger $\dot{P}$. Duncan & Lissauer (1998) show that such a planet would survive the post-main sequence mass loss. Note that reflex motion produces periodic variations on the $O - C$, which are distinguishable from parabolic variations after a significant portion of the orbit has been covered.

As discussed by Damour & Taylor (1991), any relative acceleration of the star with respect to the barycenter of the solar system will contribute to the observed $\dot{P}$. Their equations (2.2) for the differential galactic orbits, decomposed in a planar contribution (2.12), where the second term is the proper motion correction, and a perpendicular contribution (2.28), applied to G 117-B15A, show the galactic contribution to be exactly the one calculated above for proper motion, i.e., the other terms are negligible (2 to 3 orders of magnitude smaller).

6. Conclusions

We have measured the rate of change of the main pulsation period for the $T_{\rm eff} \simeq 12000$ K pulsating DA white dwarf G 117–B15A, the first ZZ Ceti to have its evolutionary rate of change measured, confirming it is the most stable optical clock known, with a rate of change of 1 s in 8.9 million years and a precise laboratory for physics at high energy. It is important to notice that mode trapping, a resonance between the local pulsation wavelength with the thickness of one of the compositional layers, can reduce the rate of period change by up to a factor of 2 (Bradley 1996), but the changes in the trapping layers are still caused by cooling.

It has taken a huge investment of telescope time to achieve such precision, but not only have we measured the cooling rate of this 400 million year old white dwarf (Wood 1995), excluding the time the star took to reach the white dwarf phase, we have also demonstrated it does not harbor planetary bodies similar to Jupiter in mass up to a distance around 30 AU from the star or smaller planets with light travel time effects on the white dwarf larger than 1s.

We claim that the 215 s periodicity in G 117-B15A is the most stable optical clock known. Santra et al. (2004) and Hoyt et al. (2005) discuss projects to build optical atomic clocks based on single trapped ions, or several laser cooled neutron atoms, of strontrium or ytterbium, expected to reach an accuracy of $\dot{P} \leq 2 \times 10^{-17}$ s/s. Considering their periods are 2.5×10^{-15} s and 1.9×10^{-13} s, even though they will be more accurate than G 117-B15A, they will be much less stable, as their timescales for period changes, $P/\dot{P}$, are 125 s and 3 h, compared to 2 Gyr for G 117–B15A. Even the Hulse & Taylor's millisecond pulsar (Hulse & Taylor 1975), has a timescale for period change of only 0.35 Gyr (Damour & Taylor 1991), but the radio millisecond pulsar PSR J1713+0747 (Splaver et al. 2005) has $\dot{P} = 8.1 \times 10^{-21}$ s/s, and a timescale of 8 Gyr, and PSR B1885+09=PSR J1857+0943 with $\dot{P} = 1.78363 \times 10^{-20}$ s/s has a stability timescale of 9.5 Gyr (Kaspi et al. 1994). Together with these millisecond pulsars, G 117–B15A may be used as the most stable known natural frequency and time-keeping standards [e.g. Kopeikin & Potapov (2004)]. The white dwarf

has the advantage of not having glitches and less severe general relativistic corrections.

It is essential to note that the measured rate of period change is consistent with the cooling rate in our white dwarf models only for cores of C or C/O. With the refinement of the models, the observed rate of period change can be used to accurately measure the ratio of carbon to oxygen in the core of this normal white dwarf, and therefore help in constraining the $C(\alpha,\gamma)O$ cross section.

This work was partially supported by grants from CNPq (Brazil), FINEP (Brazil), NSF (USA), NASA (USA). This research has made extensive use of NASA's Astrophysical Data System Abstract Service.

Table 3. Total Data Set to Date

Time of Maximum BJDD	**Epoch of Maximum**	**(O-C)** (sec)	σ (sec)	
2442397.917507	0	0.0	2.1	
2442477.797089	32071	0.5	1.7	
2442779.887934	153358	3.9	2.1	
2442783.850624	154949	1.2	2.9	
2442786.981458	156206	2.2	1.5	
2443462.962774	427607	1.6	1.4	
2443463.946592	428002	0.5	1.4	
2443465.969049	428814	0.5	1.6	
2443489.909755	438426	0.2	1.5	
2443492.898616	439626	0.9	1.6	
2443521.927837	451281	0.1	1.3	
2443552.752879	463657	0.8	1.4	
2443576.725940	473282	-1.6	3.3	
2443581.692438	475276	0.3	1.3	
2443582.693698	475678	-0.2	1.3	
2443583.697469	476081	1.0	1.3	
2443584.733602	476497	0.8	1.4	
2443604.659292	484497	1.3	1.5	
2443605.752703	484936	0.4	1.4	
2443611.693050	487321	0.6	1.3	
2443613.658222	488110	0.7	1.6	
2443636.674971	497351	8.8	3.4	
2443839.956765	578967	5.8	3.0	
2443841.976708	579778	3.7	3.5	
2443842.980413	580181	-0.7	2.2	
2443843.944332	580568	0.5	2.6	
2443869.989703	591025	1.5	2.4	
2443870.946182	591409	5.5	3.1	
2443874.916339	593003	2.4	2.1	
2443959.695117	627041	0.1	2.0	

Table 3—Continued

Time of Maximum BJDD	**Epoch of Maximum**	**(O-C)** (sec)	σ (sec)
2443963.662836	628634	1.6	2.1
2443990.664641	639475	2.7	1.3
2444169.945954	711455	0.1	1.6
2444231.822666	736298	-0.7	2.9
2444232.818992	736698	3.0	1.6
2444293.833896	761195	0.3	1.8
2444637.776174	899285	5.8	1.9
2444641.624287	900830	2.8	1.1
2444992.789531	1041820	0.1	1.6
2444994.689956	1042583	1.2	1.2
2444996.744801	1043408	2.0	1.3
2444997.723649	1043801	1.9	1.2
2445021.716661	1053434	1.7	1.4
2445703.860004	1327309	1.9	1.7
2445734.642701	1339668	2.4	1.2
2445735.643972	1340070	2.8	1.3
2446113.763716	1491882	2.9	1.2
2446443.775386	1624379	2.8	1.1
2446468.630178	1634358	2.1	1.3
2446473.718679	1636401	0.3	1.6
2446523.620086	1656436	2.2	1.6
2446524.613917	1656835	5.5	2.5
2446768.855451	1754896	2.9	1.4
2446794.935676	1765367	2.5	2.1
2446796.928219	1766167	0.3	1.6
2446797.924535	1766567	3.1	1.3
2446798.903378	1766960	2.6	1.8
2446823.663537	1776901	3.1	1.9
2446825.651132	1777699	3.7	1.5
2447231.328096	1940575	3.7	1.9

Table 3—Continued

Time of Maximum BJDD	**Epoch of Maximum**	**(O-C)** (sec)	σ (sec)
2447231.612054	1940689	5.1	3.5
2447232.396626	1941004	5.0	1.6
2447232.623291	1941095	5.9	2.9
2447233.343090	1941384	4.5	1.3
2447233.634506	1941501	4.7	2.3
2447234.319475	1941776	6.8	3.2
2447235.313250	1942175	5.2	1.4
2447235.607168	1942293	6.4	2.1
2447236.610922	1942696	6.2	1.6
2447589.375198	2084328	3.2	1.4
2447594.331735	2086318	5.2	1.6
2447595.323018	2086716	3.5	2.0
2447596.311907	2087113	10.1	2.3
2447597.315602	2087516	4.8	1.7
2447598.319339	2087919	3.1	3.1
2447499.072036	2048072	6.5	3.2
2447532.768799	2061601	1.3	1.4
2447853.846325	2190511	4.3	2.1
2447856.832697	2191710	5.2	1.9
2447918.644630	2216527	2.6	3.1
2447920.619811	2217320	6.7	3.3
2447952.622834	2230169	-3.3	2.9
2447972.620899	2238198	9.6	6.1
2447973.709340	2238635	9.7	2.6
2447973.741682	2238648	6.5	1.4
2447978.770467	2240667	10.0	2.1
2447979.781717	2241073	11.8	3.1
2447980.319627	2241289	4.6	3.5
2447977.403038	2240118	7.5	2.3
2447978.327055	2240489	4.3	3.3

Table 3—Continued

Time of Maximum BJDD	**Epoch of Maximum**	**(O-C)** (sec)	σ (sec)
2447979.358189	2240903	2.6	3.4
2447979.358145	2240903	-1.2	4.9
2447978.601069	2240599	7.4	2.5
2447980.621017	2241410	5.8	3.4
2447980.782929	2241475	7.2	2.3
2447981.325918	2241693	8.4	1.4
2447981.592393	2241800	5.7	1.4
2447981.779185	2241875	4.8	1.1
2447982.329663	2242096	7.4	1.8
2447982.743093	2242262	5.0	1.2
2447983.734400	2242660	5.4	1.2
2447979.281057	2240872	9.5	2.9
2447980.224899	2241251	-2.4	2.9
2447984.735678	2243062	6.5	1.1
2448245.724666	2347847	-3.3	5.1
2448267.799932	2356710	5.2	2.3
2448324.627972	2379526	4.3	1.2
2448325.708938	2379960	4.1	1.3
2448328.593208	2381118	6.4	1.6
2448331.661735	2382350	4.0	1.2
2448238.571479	2344975	8.3	2.2
2448622.833258	2499253	3.3	1.8
2448680.642683	2522463	6.3	1.2
2448687.614155	2525262	4.0	1.2
2448688.597979	2525657	3.4	1.2
2449062.660365	2675840	4.2	1.6
2449063.609354	2676221	6.7	1.9
2449066.615640	2677428	6.5	1.4
2449066.371558	2677330	7.2	2.0
2449066.326737	2677312	8.2	2.6

Table 3—Continued

Time of Maximum BJDD	**Epoch of Maximum**	**(O-C)** (sec)	σ (sec)
2449069.342967	2678523	6.4	1.7
2449298.239287	2770423	8.5	4.1
2449298.304041	2770449	8.2	4.1
2449294.214264	2768807	5.5	4.1
2449294.293897	2768839	-0.5	4.1
2449295.439583	2769299	-4.0	6.1
2449295.494387	2769321	-3.3	7.1
2449036.809260	2665461	2.4	2.2
2449038.677300	2666211	3.1	2.2
2449040.687310	2667018	3.6	4.1
2449041.616360	2667391	4.9	4.1
2449799.723888	2971765	5.6	1.3
2450427.920960	3223981	8.2	3.8
2450429.973242	3224805	2.7	2.4
2450430.914779	3225183	6.9	2.5
2450431.843821	3225556	7.5	1.5
2450434.912392	3226788	8.8	2.0
2450436.929828	3227598	5.4	1.7
2450483.633189	3246349	9.6	1.8
2451249.5989069	3553878	10.1	1.3
2451249.7632895	3553944	9.7	1.7
2451250.6126098	3554285	8.7	2.0
2451526.8772586	3665203	10.4	1.2
2451528.8523866	3665996	10.0	1.5
2451528.9196061	3666023	7.4	1.4
2451528.9868422	3666050	6.3	1.9
2451529.8585943	3666400	6.6	2.0
2451530.9097492	3666822	13.4	2.41
2451960.8561629	3839442	10.1	1.62
2451962.7864775	3840217	11.3	1.48

Table 3—Continued

Time of Maximum BJDD	**Epoch of Maximum**	**(O-C)** (sec)	σ (sec)
2451967.6806926	3842182	8.1	1.93
2451988.7919772	3850658	10.5	2.00
2451990.7845255	3851458	8.8	1.59
2452037.6472583	3870273	10.1	3.39
2452045.6399770	3873482	12.5	1.85
2452225.9050927	3945857	7.6	1.34
2452225.9598927	3945879	8.0	0.65
2452263.8834810	3961105	10.6	0.58
2452316.6442205	3980721	13.1	1.0
2452317.8995164	3982288	12.2	0.67
2452319.7999417	3982691	12.0	0.79
2452317.6479750	3982792	10.3	0.95
2452321.8348344	3983555	11.4	1.23
2452322.7265266	3984372	9.9	3.03
2452312.7412881	3984730	11.4	3.5
2452373.6840808	4089983	9.9	1.1
2452373.6839702	4090425	12.6	1.2
2452373.7140655	4090791	10.6	0.68
2452375.6392709	4122465	12.8	1.0
2452374.7700070	4124076	12.5	1.23
2452581.9494464	4134940	12.0	1.83
2452583.9095168	4137288	11.5	1.74
2452584.8812628	4144503	13.8	0.92
2452585.9821875	4148953	12.0	1.16
2452586.8937641	4146104	12.3	0.7
2452665.7845581	4255806	13.7	0.72
2452669.7970851	4256260	10.6	1.52
2452696.8561592	4257768	12.8	0.96
2452724.6624548	4267394	10.5	0.81
2453381.7442572	4409917	11.5	1.41

REFERENCES

Benvenuto, O. G., Córsico, A. H., Althaus, L. G., & Serenelli, A. M. 2002, MNRAS, 332, 399

Benvenuto, O. G., García-Berro, E., & Isern, J. 2004, Phys. Rev. D, 69, 082002

Bergeron, P., Wesemael, F., Lamontagne, R., Fontaine, G., Saffer, R.A., & Allard, N.F. 1995, ApJ, 449, 258

Bergeron, P., Fontaine, G., Billères, M., Boudreault, S., & Green, E. M. 2004, ApJ, 600, 404

Biesiada, M. & Malec, B. (2002) Physical Review D, 65, 43008

Bradley, P.A. 1996, ApJ, 468, 350

Bradley, P. A., & Winget, D. E. 1991, ApJS, 75, 463

Bradley, P. A. 1998, ApJS, 116, 307

Brassard, P., Fontaine, G., Wesemael, F., & Talon, A. 1993, In White Dwarfs: Advances in Observation and Theory, ed. M.A. Barstow, (Dordrecht: Kluwer), 485

Brassard, P., Fontaine, G., Wesemael, F., & Tassoul, M. 1992, ApJS, 81, 747

Córsico, A.H., Benvenuto, O.G., Althaus, L.G., Isern, J. & Garcia-Berro, E. 2001, New Astronomy, 5, 197.

Costa, J. E. S., Kepler, S. O., & Winget, D. E. 1999, ApJ, 522, 973

Cutri, R. M., et al. 2003, VizieR Online Data Catalog, 2246, 1

Damour, T., & Taylor, J. H. 1991, ApJ, 366, 501

Table 3—Continued

Time of Maximum BJDD	**Epoch of Maximum**	**(O-C)** (sec)	σ (sec)	
2453439.7653860	4433212	13.9	1.0	
2453446.6073830	4435959	15.2	0.71	
2453473.6191370	4446804	15.1	0.75	

Duncan, M. J., & Lissauer, J. J. 1998, Icarus, 134, 303

Eggen, O.J., and Greenstein, J.L. 1965, ApJ, 141, 183

Finley, D. S., Koester, D., & Basri, G. 1997, ApJ, 488, 375

Fontaine, G., Brassard, P., & Bergeron, P. 2001, PASP, 113, 409

Giclas, H. L., Burnham, R., & Thomas, N. G. 1963, Lowell Observatory Bulletin, Vol.6, 120, 42

Greaves, J. 2004, MNRAS, 355, 585

Harrington, R.S. & Dahn, C.C. 1980, AJ, 85, 454

Hawley, S. L., et al. 2002, AJ, 123, 3409

Holberg, J. B., Barstow, M. A., & Burleigh, M. R. 2003, ApJS, 147, 145

Hoyt, C. W., Barber, Z. W., Oates, C. W., Fortier, T. M., Diddams, S. A., & Hollberg, L. 2005, ArXiv Physics e-prints, arXiv:physics/0503240

Hulse, R. A., & Taylor, J. H. 1975, ApJ, 195, L51

Isern, J., Garcia-Berro, E., Corsico, A. H., Benvenuto, O. G., & Althaus, L. G. 2004, Communications in Asteroseismology, 145, 13

Kaspi, V. M., Taylor, J. H., & Ryba, M. F. 1994, ApJ, 428, 713

Kawaler, S. D., Winget, D. E., Iben, I., & Hansen, C. J. 1986, ApJ, 302, 530

Kepler, S. O., Robinson, E. L., & Nather, R. E. 1983, ApJ, 271, 744

Kepler, S.O. 1984, ApJ, 286, 314

Kepler, S.O. 1993, Baltic Astronomy, 2, 515

Kepler, S.O., Robinson, E.L., Nather, R.E., & McGraw, J.T. 1982, ApJ, 254, 676

Kepler, S.O., et al. 1991, ApJ, 378, L45.

Kepler, S.O., et al. 1995, Baltic Astronomy, 4, 221.

Kepler, S.O. et al. 2000, ApJ, 534, L185.

Kepler, S. O. 2004, International Journal of Modern Physics D, 13, 1493

Kleinman, S. J., et al. 2004, ApJ, 607, 426

Koester, D., Allard, N.F., & Vauclair, G. 1994, A&A, 291, L9

Koester, D., & Holberg, J. B. 2001, ASP Conf. Ser. 226: 12th European Workshop on White Dwarfs, 226, 299

Kopeikin, S. M., & Potapov, V. A. 2004, MNRAS, 355, 395

Kotak, R., van Kerkwijk, M. H., & Clemens, J. C. 2004, A&A, 413, 301

Lamb, D. Q., & van Horn, H. M. 1975, ApJ, 200, 306

Lang, K.R. 1991, Astrophysical Data: Planets and Stars, (Springer-Verlag, NY), p. 145

Mestel, L. 1952, MNRAS, 112, 583

McGraw, J.T. 1979, ApJ, 229, 203

McGraw, J.T., & Robinson, E.L. 1976, ApJ, 205, L155

Montgomery, M. H. & Winget, D. E. 1999, ApJ, 526, 976.

Mullally, F., Thompson, S. E., Castanheira, B. G., Winget, D. E., Kepler, S. O., Eisenstein, D. J., Kleinman, S. J., & Nitta, A. 2005, ApJ, 625, 966

Mukadam, A. S., et al. 2003, ApJ, 594, 961

Mukadam, A. S., et al. 2004, ApJ, 607, 982

Mukadam, A. S., Winget, D. E., von Hippel, T., Montgomery, M. H., Kepler, S. O., & Costa, A. F. M. 2004, ApJ, 612, 1052

Munn, J. A., et al. 2004, AJ, 127, 3034

O'Donoghue, D. 1994, MNRAS, 270, 222

Nather, R.E., Winget, D.E., Clemens, J.C., Hansen, C.J., & Hine, B.P. 1990, ApJ, 361, 309

Nather, R. E. & Mukadam, A. S. 2004, ApJ, 605, 846

Pajdosz, G. 1995, A&A, 295, L17.

Panei, J. A., Althaus, L. G., & Benvenuto, O. G. 2000, A&A, 353, 970

Pickles, A. J. 1998, PASP, 110, 863

Robinson, E.L. 1979, in Proc. of IAU Colloq. 53, White Dwarfs and Variable Degenerate Stars, ed. H.M. Van Horn & V. Weidemann (Rochester: Univ. Rochester), 343

Robinson, E.L., Kepler, S.O., & Nather, R.E. 1982, ApJ, 259, 219

Robinson, E.L., Mailloux, T.M., Zhang, E., Koester, D., Stiening, R.F., Bless, R.C., Percival, J.W., Taylor, M.J., & van Citters, G.W. 1995, ApJ, 438, 908

Santra, R., Arimondo, E., Ido, T., Greene, C. H., & Ye, J. 2004, ArXiv Physics e-prints, arXiv:physics/0411197

Silvestri, N. M., Oswalt, T. D., & Hawley, S. L. 2002, AJ, 124, 1118

Splaver, E. M., Nice, D. J., Stairs, I. H., Lommen, A. N., & Backer, D. C. 2005, ApJ, 620, 405

Standish, E. M. 1998, A&A, 336, 381

Standish, E. M. 2004, A&A, 417, 1165

van Altena, W. F., Lee, J. T., & Hoffleit, E. D. 1995, New Haven, CT: Yale University Observatory, —c1995, 4th ed., stars 2232.01.

van Altena, W. F., Lee, J. T., & Hoffleit, E. D. 2001, VizieR Online Data Catalog, 1238, stars USNO 479 and 480.

Winget, D. E., van Horn, H. M., & Hansen, C. J. 1981, ApJ, 245, L33

Winget, D. E., Hansen, C. J., & van Horn, H. M. 1983, Nature, 303, 781

Winget, D. E., Hansen, C. J., Liebert, J., van Horn, H. M., Fontaine, G., Nather, R. E., Kepler, S. O., & Lamb, D. Q. 1987, ApJ, 315, L77

Winget, D. E., Kepler, S. O., Kanaan, A., Montgomery, M. H., & Giovannini, O. 1997, ApJ, 487, L191.

Wood, M. A. 1995, LNP Vol. 443: White Dwarfs, 41

Wood, M. A., & Winget, D. E. 1988, Multimode Stellar Pulsations, 199

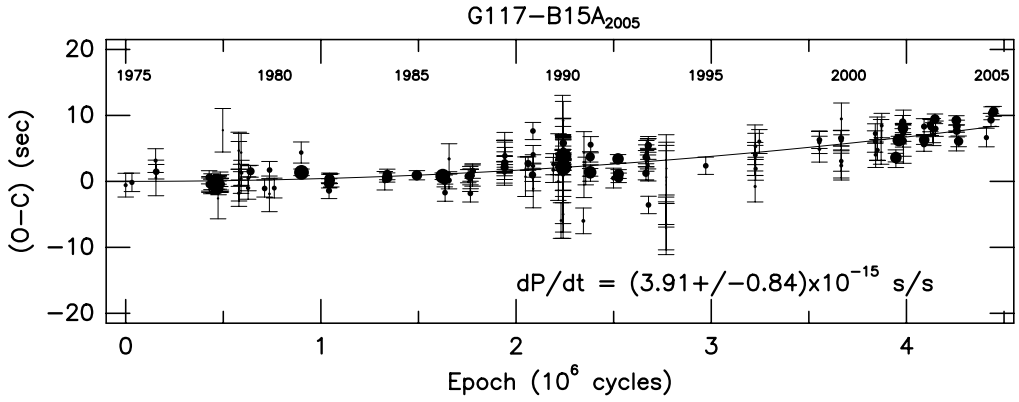

Fig. 1.— **(O-C)**: (**O**bserved minus **C**alculated times of maxima) for the 215 s pulsation of G 117-B15A. The size of each point is proportional to its weight, i.e., inversely proportional to the uncertainty in the time of maxima squared. We show 2σ error bars for each point, and the line shows our best fit parabola to the data. The error bars plotted are those before adding the external uncertainty of 1s quadratically, discussed in the text. The fact the line does not overlap these error bars are a demonstration they are underestimate. Note that as the period of pulsation is 215.197s, the whole plot shows only ± 36 deg in phase.

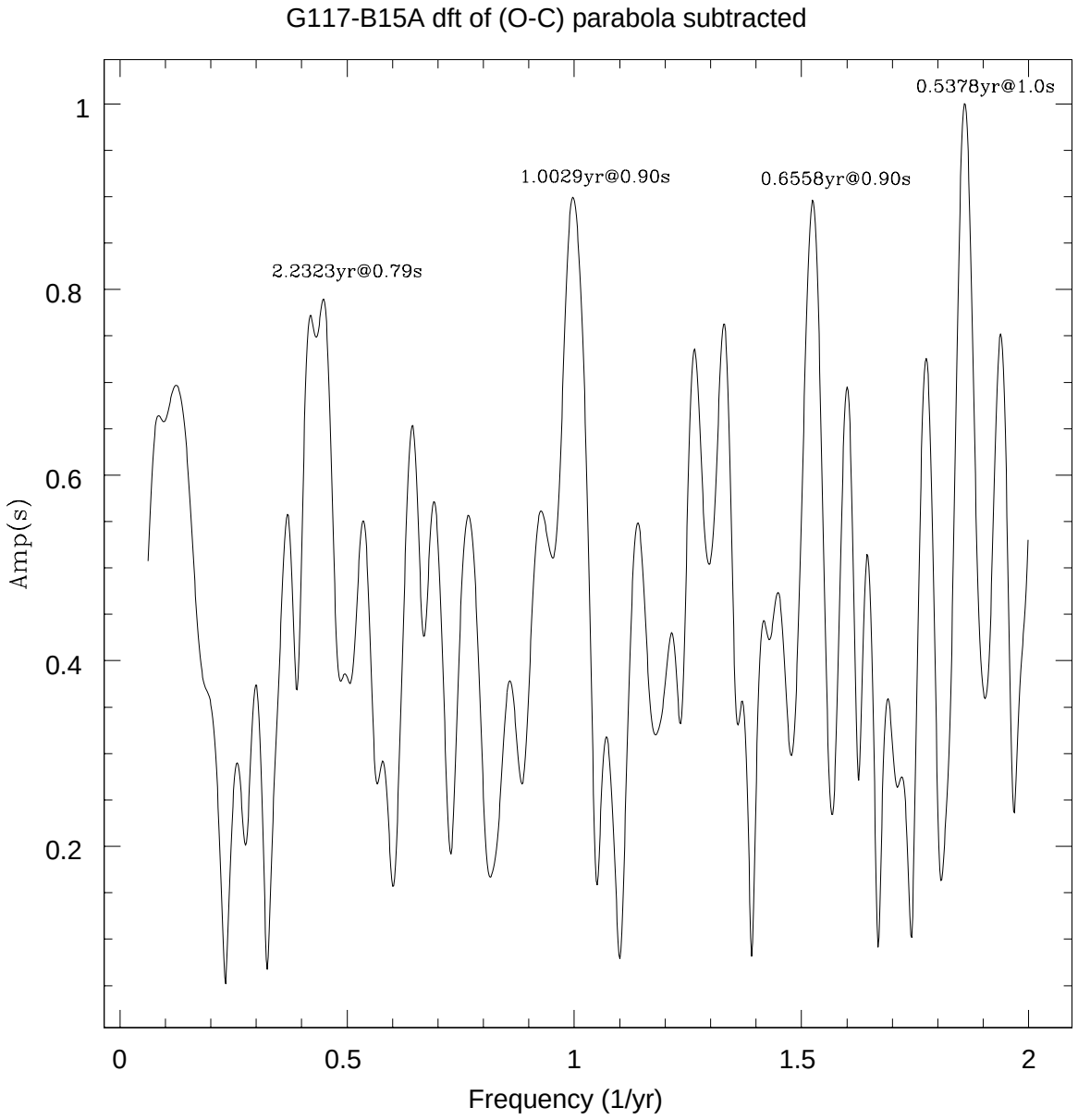

Fig. 2.— Fourier transform of the (O-C): (**O**bserved minus **C**alculated times of maxima) for the 215 s pulsation of G 117-B15A, after we subtract the parabola. Kepler's law (1616) shows that $a_* \simeq \frac{M_P}{M_*^{2/3}} \left(\frac{G}{4\pi^2}\right)^{1/3} P^{2/3}$, considering $M_P \ll M_*$, from which we get a_*(light-second) $\simeq 0.565 \frac{M_P}{M_J} P^{2/3}$(yr) i.e., a 1s light travel time, as the limit shows, for planets with masses between 1.6 M_J and 0.27 M_J=87 $M_\oplus$, for periods between 6 months and 7 yr, respectively. The highest peak, at a frequency of 1.85 yr^{-1}, corresponding to a period of 6.5 months, is extremely hard to study in our data set, as we normally observe for only 3 months separated by 1 year. These variations can be caused by beating of very closely spaced pulsations (Kepler et al. (1995)), and we must take into account that multiplets cause non-sinusoidal variations, as the triplet in G 226-29 studied by Kepler et al. (1983).

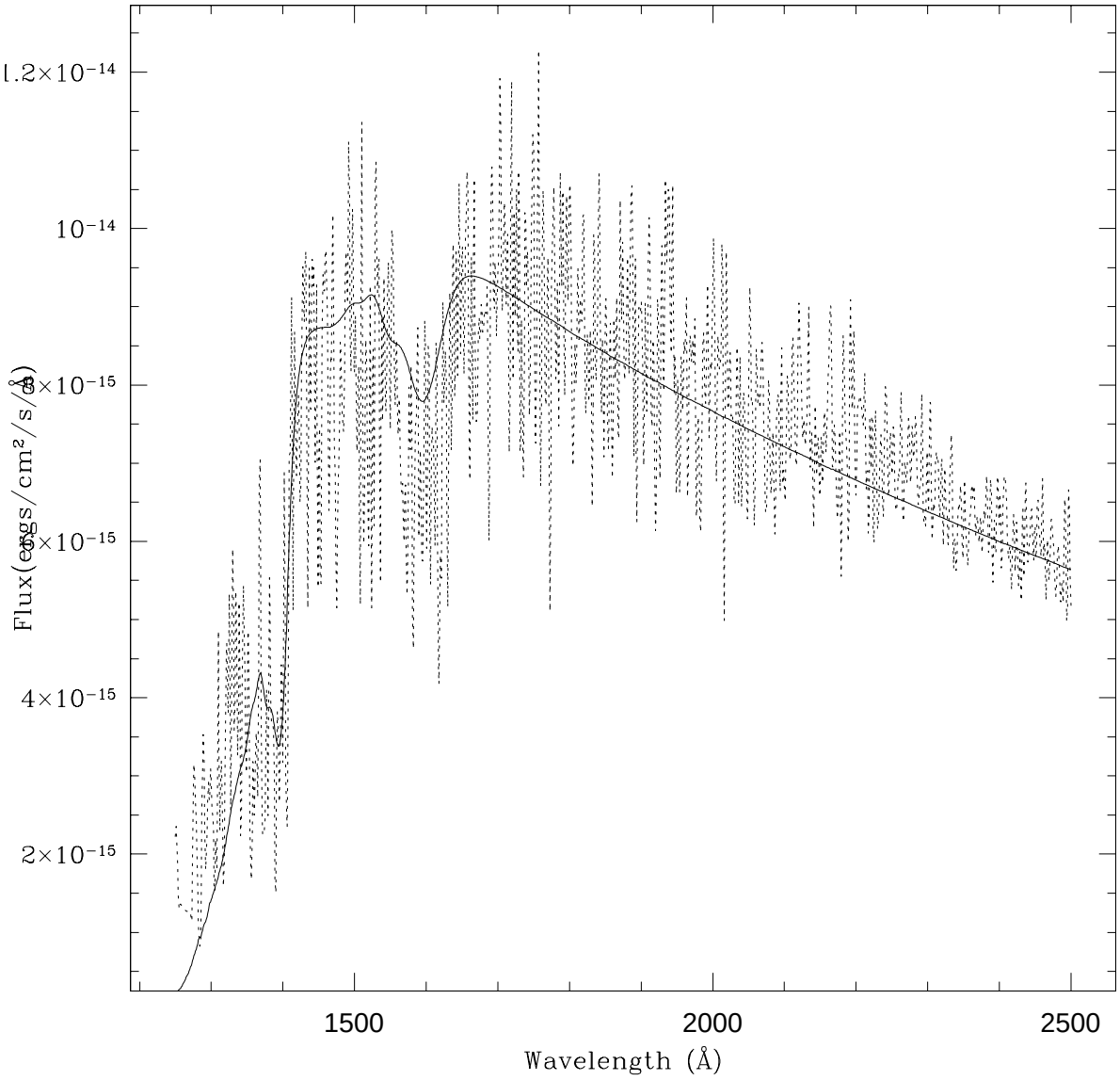

Fig. 3.— Fit of a model atmosphere with $T_{\rm eff} = 12\,000\,{\rm K}$, $\log g = 8.0$, d=67 pc, to the HST FOS spectra of G 117-B15A.

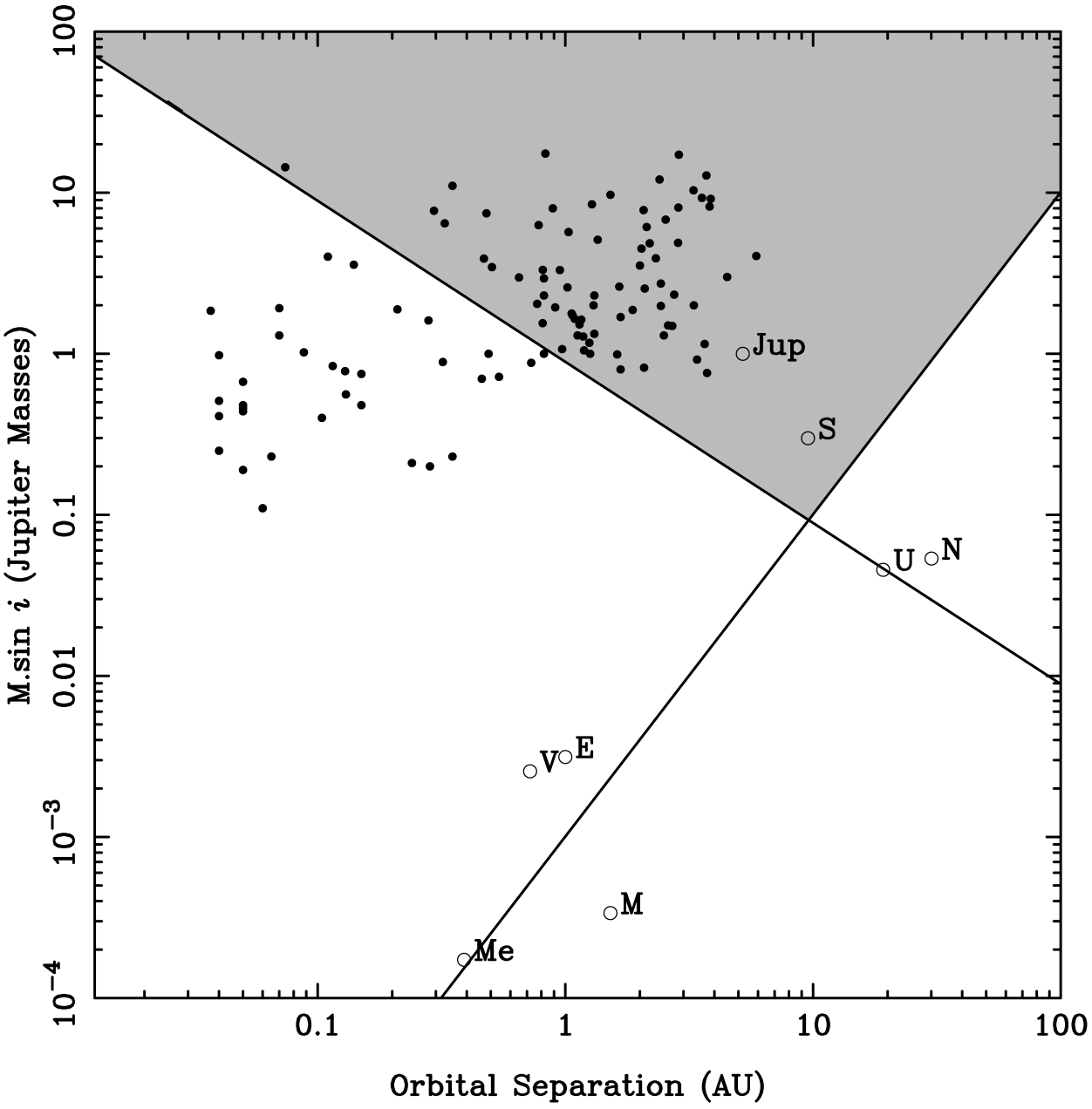

Fig. 4.— Planet exclusion region around G117-B15A. The filled dots represent known extra-solar planets around their stars, while the open circles represent solar system planets around the Sun. The short period limit is the limit on the mass of a planet that would produce a peak in the Fourier transform smaller than those seen in Fig. 2. The long period limit is the mass limit of a companion that would account for the observed $\dot{P}$. Any planet above both lines would have been detected.